MIT Open Access Articles

Handling Initial Conditions in Vector Fitting for Real Time Modeling of Power System Dynamics

Massachusetts Institute of Technology

Handling Initial Conditions in Vector Fitting for Real Time Modeling of Power System Dynamics

Tommaso Bradde [1] , **Samuel Chevalier** [2,*] , **Marco De Stefano** [1] , **Stefano Grivet-Talocia** [1] and **Luca Daniel** [3]

1   Department of Electronics and Telecommunications, Politecnico di Torino, 10129 Torino, Italy; tommaso.bradde@polito.it (T.B.); marco.destefano@polito.it (M.D.S.); stefano.grivet@polito.it (S.G.-T.)
2   Department of Electrical Engineering, Technical University of Denmark, 2800 Kgs. Lyngby, Denmark
3   Department of Electrical Engineering and Computer Science, Massachusetts Institute of Technology, Cambridge, MA 02142, USA; luca@mit.edu
*   Correspondence: schev@elektro.dtu.dk

Abstract: This paper develops a predictive modeling algorithm, denoted as Real-Time Vector Fitting (RTVF), which is capable of approximating the real-time linearized dynamics of multi-input multi-output (MIMO) dynamical systems via rational transfer function matrices. Based on a generalization of the well-known Time-Domain Vector Fitting (TDVF) algorithm, RTVF is suitable for online modeling of dynamical systems which experience both initial-state decay contributions in the measured output signals and concurrently active input signals. These adaptations were specifically contrived to meet the needs currently present in the electrical power systems community, where real-time modeling of low frequency power system dynamics is becoming an increasingly coveted tool by power system operators. After introducing and validating the RTVF scheme on synthetic test cases, this paper presents a series of numerical tests on high-order closed-loop generator systems in the IEEE 39-bus test system.

Keywords: power system dynamics; real-time modeling; vector fitting

1. Introduction

Due to the aggressive deployment of Wide Area Monitoring Systems (WAMS), a deluge of time series data streams are emerging from modernizing smart grids. For instance, as of 2017, Operating Procedure No. 22 specifies that all generation above 100 MW in the ISO New England system must provide Phasor Measuring Unit (PMU) observability at the point of interconnection [1]. Similarly, the 2018 Nodal Operating Guide specifies that all new generators above 20MVA in the ERCOT (Texas) system must provide PMU observability [2]. In order to both capitalize on these data streams and enforce effective dynamic security assessment (DSA) in the face of a rapidly modernizing energy landscape with shrinking inertia margins [3], the North American Electric Reliability Corporation (NERC) has recently implemented new directives [4] which mandate the continual development of static and dynamic network planning models. The simulated response of these models must be compared to actual time series data collected in the network to validate their accuracy [5]. Associated procedures must also resolve model prediction aberrations. Traditional "staged" testing of grid models can be costly and inconvenient, because generators must go offline [6]. Thus, performing model tuning and validation online is particularly valuable.

Furthermore, real-time modeling of the grid's dynamics at a "wide-area" level can provide useful operational benefits, such as modal damping ratio monitoring and controller tuning. For instance, the 3.1 GW Pacific DC Intertie (PDCI) line in the Western United States has been recently outfitted with a damping controller to increase its transfer capabilities [7]. This celebrated controller is tuned using an open loop transfer function model of the power system which was empirically measured via intrusive multi-sine modulation of the HVDC

power controllers [8]. Methods for online modeling of these types of dynamics, therefore, could allow for enhanced controller tuning across many wide area applications.

In the electromechanical frequency range, power system dynamics are still dominated by synchronous generators [3]. A wealth of literature exists on the nonlinear physical modeling of these generators, their associated high-order controllers, and the networks to which they interconnect [9,10]. Applying, tuning, and validating these models in the context of large realistic power systems faces a variety of practical obstacles; these include the exclusion of unmodeled dynamics, measurement noise, uncertain physical parameter values, unknown controller changes, and, in the limiting case of linearized modeling, residual nonlinearities and drifting equilibrium points. In recent years, a variety of methods have been proposed for the purpose of identifying, validating and tuning these models [4,6,11–14], usually via Kalman filter-based parameter tuning and "play-back" simulation. The vast majority of the proposed modeling and validation algorithms are characterized by two salient features. First, they are parameterized by a physical prior; that is, they leverage the structure of a given physical model which can assumably be tuned to explain the full set observed dynamics. Second, they are typically designed to be deployed in the presence of a sufficiently strong network perturbation (e.g., ground fault). Together, these assumptions allow for a variety of helpful simplifications, such as initial state decay negligence and high-fidelity prior availability. Such algorithmic features can be burdensome if the prior model is incomplete or if real-time modeling updates are desired.

Predictive modeling algorithms which are free from these limitations can provide a variety of advantages. If power system modeling can be performed by a parameterized "black box" approximation, then the associated algorithm will be freed from the constraints of a potentially erroneous, or completely unknown, prior model. Additionally, if this algorithm can be implemented in the face of ambient, rather than severe, operating conditions, then updates can be performed on the fly. There is a large collection of well-cited literature devoted to the creation of linear dynamical black box models from time series data in power systems, primarily at the "wide area" level, but also at the individual generator level. Excellent reviews on the topic are provided in [15,16]. One of the most popular "modal identification" methods, known as Prony analysis, was first applied to power systems in 1990 [17]. It was further shown in [18] that Prony analysis applied to transient data and Wiener-Hopf linear prediction applied to ambient data could both identify very similar system dynamics. Subsequent publications further refined these methods [19,20], but most of them were focused on identification of system modes (i.e., poles), rather than the full transfer functions. More recent work has focused on building model reduced transfer functions from measured terminal data. Using a simple autoregressive with exogenous input (ARX) model, [21] develops a process for computing a dynamic equivalent transfer function with simulated or measured data. Voltage magnitude and frequency are chosen as inputs, while active and reactive power flows across lines are chosen as outputs. MIMO transfer function approaches are developed in [22], where poles, zeros, and model order are iteratively perturbed based on a least-squares numerical procedure inside a standard MATLAB toolbox.

Most recently, vector fitting approaches have been leveraged to construct power system models from measured field data. In [23], authors use the numerical Laplace transform to push the problem into the frequency domain. Next, vector fitting and relative dominant-pole measurements (RDPMs) are iteratively leveraged to build estimations of wide area system modes. Similarly, [24] combines time domain vector fitting and the popular ring down analysis to develop a novel modal estimation routine. In a more generic application, [25] uses out-of-the-box TDVF to construct a SISO linear model of a turbine governor system from measured PMU; droop gain values are then captured from the constructed model.

The black-box identification of dynamic models from time series data goes far beyond power system applications and is regarded as a well established field [26,27]; popular algorithms include the Multivariable Output Error State Space (MOESP) and Numerical

algorithms for Subspace State Space System Identification (N4SID) techniques [28]. As noted, one prominent approach is the Time-Domain Vector Fitting (TDVF) scheme [26,29, 30]. This approach is applicable for estimating rational models of linear systems, starting from the time domain samples of input and output data. Unfortunately, canonical TDVF has the following restrictions:

- The system must be at rest when the data acquisition begins. This guarantees that the input and output data are related by a linear transfer function with no contribution from the zero-input (i.e. initial state decay) response.
- For a MIMO system with P ports, only separate modeling of each column of the transfer matrix is possible. This limitation requires that only one of the P input components is acting on the system during the separate modeling periods for each transfer matrix column.

Since online modeling typically requires the unknown system to be characterized (i) during its dynamic evolution and (ii) in the presence of concurrently acting inputs, the above limitations often make TDVF unsuitable for real-time MIMO applications. This is especially true in the case of electrical power systems. Due to constant load switching and system perturbations, the system never reaches a truly steady state condition. Thus, any measured signals from the system will always contain some degree of initial state decay. Furthermore, generic subsystems of three-phase AC power systems are inherently MIMO in nature [31], with orthogonal input signals (e.g., voltage magnitude and voltage phase) which are always applied in a concurrent manner. This is still true, even when a symmetric three-phase power system is collapsed down to a so-called single-line diagram. Since single-line diagrams are modeled using a quasi-stationary (e.g., sinusoidal) phasor approximation [9], there are always two components associated with the input and output signals at the terminal of any power system component. In this quasi-stationary context, only under very special symmetry conditions can a MIMO transfer function be fully represented as a SISO transfer function [31].

In order to address the aforementioned limitations of canonical TDVF, this paper introduces a generalized vector fitting extension, known as Real-Time Vector Fitting (RTVF). The remainder of this paper is organized as follows. In Section 2, we recall the basic TDVF scheme in order to provide a framework on which the proposed approach is built. We then present our key contributions, namely:

1. We remove the restrictions of the basic TDVF scheme by proposing a new problem setting (Section 3).
2. We develop a first generalization of the basic TDVF scheme by removing the requirement of pure zero-state conditions, hence allowing for the presence of non-vanishing initial conditions (Section 4).
3. We develop a second generalization by allowing all input components to act concurrently in the time series data sets used to train the RTVF model (Section 5).

In Section 6, we provide implementation details. Numerical test results, based on both synthetic and realistic power system models, are given in Section 7.

2. Technical Background

2.1. Notation

We denote a generic scalar as x, a generic vector as $\boldsymbol{x}$ or $\boldsymbol{X}_0$, and a generic matrix as $\mathbf{X}$. The identity matrix is denoted as $\mathbf{I}$, with size inferred from the context. We use the symbol s for the complex frequency (Laplace) variable; $\mathbb{R}$ and $\mathbb{C}$ represent the sets of real and complex numbers, respectively.

We consider a possibly nonlinear dynamic system $\mathcal{S}$ with input and output signals denoted as $\boldsymbol{u}(t) \in \mathbb{R}^P$ and $\boldsymbol{y}(t) \in \mathbb{R}^P$, respectively. For later use, we denote with $\boldsymbol{x}(t) \in \mathbb{R}^{\bar{N}}$ some unknown system state vector, although we assume no information on the internal

system representation. We assume instead that a measurement tool is available that returns K samples of time-domain input-output vectors

$$\boldsymbol{u}(t_k), \boldsymbol{y}(t_k) \quad k = 1, ..., K \tag{1}$$

acquired at sampling rate F_s. Without loss of generality, we set $t_1 = 0$ throughout this paper. All derivations will hold true for $t_1 \neq 0$, provided the time variable is redefined as $t \leftarrow t - t_1$.

2.2. The Standard Setting for Data-Driven Modeling

When the underlying system $\mathcal{S}$ is Linear and Time-Invariant (LTI), Laplace-domain input and output signals are related by

$$\boldsymbol{Y}(s) = \check{\mathbf{H}}(s)\boldsymbol{U}(s). \tag{2}$$

An estimate $\mathbf{H}(s)$ of the true transfer function $\check{\mathbf{H}}(s)$ can be determined from the samples (1) through one of the several available data-driven model order reduction methods. In particular, the TDVF scheme [26,29,30] considered in this work assumes that the system is initially at rest, and the *initial conditions* vanish identically as

$$\boldsymbol{u}(0) \equiv \mathbf{0}, \quad \boldsymbol{y}(0) \equiv \mathbf{0}, \quad \boldsymbol{x}(0) \equiv \mathbf{0}. \tag{3}$$

This setting guarantees that only the zero-state response contribution is present in the output samples.

2.3. Time-Domain Vector Fitting

The basic TDVF scheme assumes availability of

- time series of each output $y_{ij}(t)$ at port i excited by a single input $u_j(t)$ placed at port j and acting alone, with $u_{k \neq j} = 0$; this requirement imposes a restriction on the training sequences that can be used for model extraction;
- some initial estimate of the dominant system poles $\{q_n, n = 1, \dots, N\}$. Usually, such poles are initialized as random real or complex conjugate pairs with $\text{Re}\{q_n\} < 0$ and $|q_n| < \Omega$, where Ω is the modeling bandwidth of interest [26,32].

Based on the training data, TDVF constructs the approximation

$$d_0 \cdot y_{ij}(t) + \sum_{n=1}^{N} d_n \cdot y_{ij}^{(n)}(t) \approx c_{ij}^{(0)} \cdot u_j(t) + \sum_{n=1}^{N} c_{ij}^{(n)} \cdot u_j^{(n)}(t) \tag{4}$$

for $t = t_k$ with $k = 1, \dots, K$, where $c_{ij}^{(n)}$ and d_n are unknown coefficients to be determined via a linear least squares solution. In (4), superscript $^{(n)}$ denotes the result obtained by the single-pole filter (i.e., convolution) via

$$z^{(n)}(t) = \int_0^t e^{q_n(t-\tau)} z(\tau) d\tau \tag{5}$$

on any arbitrary signal $z(t)$ with $z(0) = 0$. The regression problem (4) corresponds to the frequency-domain relation

$$Y_{ij}(s) \approx H_{ij}(s)\, U_j(s) \approx \frac{c_{ij}^{(0)} + \sum_{n=1}^{N} \dfrac{c_{ij}^{(n)}}{s - q_n}}{d_0 + \sum_{n=1}^{N} \dfrac{d_n}{s - q_n}} \cdot U_j(s) \tag{6}$$

which provides an element-wise rational approximation $H_{ij}(s) \approx \check{H}_{ij}(s)$ written in barycentric form. The initial poles q_n in (6) cancel out, and the actual poles of $H_{ij}(s)$ correspond to the zeros z_n of the denominator

$$D(s) = d_0 + \sum_{n=1}^{N} \frac{d_n}{s - q_n}. \tag{7}$$

Problem (4) is solved iteratively, by using these zeros as starting poles for the next iteration via $q_n \leftarrow z_n$. Iterations stop when the poles and/or the least-squares residual (fitting error) stabilize [26,33], or alternatively when a maximum number of iterations $\nu_{\max}$ is reached.

3. A New Problem Setting for TDVF

Let us now consider system $\mathcal{S}$ operating in real time, with input and output measured signals (1) collected during system operation. Since data recording may start at an arbitrary time instant when system is not at rest, the output samples $y(t)$ may include contributions from both the zero-input and the zero-state response, implying that all initial conditions cannot be considered as vanishing as in (3). Moreover, all input channels are expected to be active concurrently. Therefore, the basic TDVF assumptions do not hold and need a generalization.

From now on, we assume a mildly nonlinear systems $\mathcal{S}$, whose dynamics can be approximated [34] by splitting inputs, outputs and states as

$$\begin{aligned} u(t) &= U_0 + \widetilde{u}(t), \\ y(t) &= Y_0 + \widetilde{y}(t), \\ x(t) &= X_0 + \widetilde{x}(t), \end{aligned} \tag{8}$$

where

$$U_0 = u(0), \quad X_0 = x(0), \quad Y_0 = y(0) \tag{9}$$

are regarded as *non-necessarily* vanishing initial conditions. The evolution of the *small-signal* components $\widetilde{u}(t)$, $\widetilde{y}(t)$, $\widetilde{x}(t)$ can be accurately related by an LTI operator with transfer function $\check{H}(s)$. Our main objective is to devise a numerical scheme that, based on the samples (1), returns an estimate $\mathbf{H}(s) \approx \check{\mathbf{H}}(s)$ of the small-signal transfer function. This objective is attained by exploiting two generalizations of the basic TDVF scheme:

1. We remove the requirements of pure zero-state conditions by allowing for the presence of nonvanishing initial conditions (9). This problem is addressed in Section 4.
2. We allow for all input components u_j acting concurrently in the training time series, as in common system operation conditions. This problem is addressed in Section 5.

4. Handling Initial Conditions

In this section, we formulate a generalized identification problem that provides an estimate $\mathbf{H}(s)$ of the small-signal transfer function, assuming non-vanishing initial conditions. Although initial conditions U_0, Y_0 are known from the training data, no information on the initial state X_0 is available. Thus, a direct decomposition of $y(t)$ into its zero-state and zero-input contributions is generally not possible. This section provides theoretical justification for the proposed RTVF formulation of Section 5 and may be skipped at first reading.

In order to characterize the role of the unknown initial state, we first consider a generic LTI system in state-space form:

$$\begin{aligned} \dot{x}(t) &= \mathbf{A}x(t) + \mathbf{B}u(t), \\ y(t) &= \mathbf{C}x(t) + \mathbf{D}u(t), \end{aligned} \tag{10}$$

with the only restriction that $\mathbf{A}$ should be nonsingular. Inserting the signal decomposition (8) into (10) leads to

$$\dot{x}(t) = \dot{\tilde{x}}(t) = \mathbf{A}(X_0 + \tilde{x}(t)) + \mathbf{B}(U_0 + \tilde{u}(t)) \tag{11}$$

$$\tilde{y}(t) + Y_0 = \mathbf{C}(X_0 + \tilde{x}(t)) + \mathbf{D}(U_0 + \tilde{u}(t)). \tag{12}$$

The output (12) can be equivalently rewritten by splitting the constant and the time-varying small-signal components as

$$Y_0 = \mathbf{C}X_0 + \mathbf{D}U_0, \tag{13}$$

$$\tilde{y}(t) = \mathbf{C}\tilde{x}(t) + \mathbf{D}\tilde{u}(t), \quad \forall t \geq 0. \tag{14}$$

Two scenarios are possible:

1. The system is at constant steady-state for $t = 0$ (equivalently, $\forall t \leq 0$). This scenario is common in electronic circuit simulation, where a constant bias is applied first and all initial conditions are found; transient analysis is performed next, starting from the computed initial conditions. Since electrical power systems never reach steady state, this condition can never be exploited in practice. Under this assumption, all small-signal components vanish for $t \leq 0$. Therefore, (11) reduces to

$$\mathbf{A}X_0 + \mathbf{B}U_0 = 0 \quad \rightarrow \quad X_0 = -\mathbf{A}^{-1}\mathbf{B}U_0 \tag{15}$$

and provides the initial state condition X_0. Since $\mathbf{A}$ is nonsingular, the system has no poles at the origin and supports constant steady-state operation. Combining (11) with (15), for $t > 0$, the small-signal components fulfill the standard dynamic equation

$$\dot{\tilde{x}}(t) = \mathbf{A}\tilde{x}(t) + \mathbf{B}\tilde{u}(t). \tag{16}$$

Combining (14) and (16) provides the small-signal transfer function $\check{\mathbf{H}}(s)$ in terms of the state-space matrices:

$$\check{\mathbf{H}}(s) = \mathbf{C}(s\mathbf{I} - \mathbf{A})^{-1}\mathbf{B} + \mathbf{D} = \frac{\check{\mathbf{N}}(s)}{\check{D}(s)} \tag{17}$$

with $\check{D}(s) = |s\mathbf{I} - \mathbf{A}|$. Identification of a rational model for $\check{\mathbf{H}}(s)$ can be performed by subtracting the initial conditions U_0, Y_0 from the input and output signals and then applying a zero-state identification scheme, such as basic TDVF, to small-signal components $\tilde{u}(t)$, $\tilde{y}(t)$.

2. The second scenario is relevant for our application, and it corresponds to the case where the system is *not* operating under constant steady-state conditions for $t < 0$. In this setting, (15) does not hold and

$$X_0 \neq -\mathbf{A}^{-1}\mathbf{B}U_0. \tag{18}$$

Therefore, even if the initial conditions U_0, Y_0 are removed from the input and output signals, the corresponding small-signal output $\tilde{y}(t)$ still includes a contribution from the initial state. This contribution is analyzed next.

Characterization of Residual Zero-Input Contributions

Assuming that U_0 and X_0 are known, system evolution in terms of small-signal state components is obtained by integrating the dynamic Equation (11) for $t > 0$ as

$$\tilde{x}(t) = \int_0^t e^{\mathbf{A}(t-\tau)}(\mathbf{B}\tilde{u}(\tau) + \mathbf{A}X_0 + \mathbf{B}U_0)d\tau. \tag{19}$$

Simple algebraic manipulations allow us to rewrite (19) as

$$\widetilde{x}(t) = \int_0^t e^{\mathbf{A}(t-\tau)}\mathbf{B}\widetilde{u}(\tau)d\tau + \left[e^{\mathbf{A}t} - \mathbf{I}\right]\underbrace{(X_0 + \mathbf{A}^{-1}\mathbf{B}U_0)}_{T_0}, \tag{20}$$

where the contribution of the initial state condition is explicit. Note that, in case of steady-state operation for $t < 0$, the second term in (20) vanishes since $T_0 = \mathbf{0}$, and the corresponding solution reduces to the solution of the small-signal system (16). The term T_0 can thus be considered as the difference between the actual initial state X_0 and the constant state that would be obtained if the system were operating under steady-state conditions excited by the constant input U_0.

Taking the Laplace transform of (20) yields

$$\widetilde{X}(s) = (s\mathbf{I} - \mathbf{A})^{-1}\mathbf{B}\,\widetilde{U}(s) + \left[(s\mathbf{I} - \mathbf{A})^{-1} - s^{-1}\mathbf{I}\right]T_0. \tag{21}$$

Inserting (21) into the output equation (14) leads to

$$\widetilde{Y}(s) = \mathbf{C}\widetilde{X}(s) + \mathbf{D}\widetilde{U}(s) = \check{\mathbf{H}}(s)\widetilde{U}(s) + \mathbf{\Gamma}_0(s), \tag{22}$$

where $\check{\mathbf{H}}(s)$ is given by (17). Additionally,

$$\mathbf{\Gamma}_0(s) = (\mathbf{C}(s\mathbf{I} - \mathbf{A})^{-1} - s^{-1}\mathbf{C})\,T_0 = \frac{\check{G}(s)}{s \cdot \check{D}(s)}, \tag{23}$$

where $\check{G}(s)$ is an unknown polynomial vector. Relation (22) is therefore equivalent to

$$\widetilde{Y}(s) = \frac{\check{\mathbf{N}}(s)}{\check{D}(s)}\,\widetilde{U}(s) + \frac{\check{G}(s)}{s \cdot \check{D}(s)}\,. \tag{24}$$

The two terms in (24) share the same denominator $\check{D}(s)$ up to a pole at $s = 0$, which represents the constant contribution of the non-vanishing initial conditions. This observation is the key enabling factor for building a self-consistent vector fitting scheme to estimate model $\mathbf{H}(s) \approx \check{\mathbf{H}}(s)$, as it properly takes into account the presence of the additional term $\mathbf{\Gamma}_0(s)$ in (22).

5. The Real-Time Vector Fitting Scheme

In this section, we propose our Real-Time Vector Fitting (RTVF) scheme. In particular, our key idea and the proposed generalizations follow:

1. The key idea of our method consists of adding to the standard rational transfer function expression an extra term that shares the same denominator $D(s)$ plus a pole at $s = 0$, representing the constant contribution of the non-vanishing initial conditions.

$$\widetilde{Y}(s) \approx \frac{\mathbf{N}(s)}{D(s)}\,\widetilde{U}(s) + \frac{G(s)}{s \cdot D(s)}\,. \tag{25}$$

2. Since polynomials $\mathbf{N}(s)$ and $D(s)$ are typically expanded in a standard barycentric form as in (6) using an initial pole set q_n, we propose the use of a similar expansion for the components of the unknown vector $G(s)$:

$$G_i(s) = b_i^{(0)} + \sum_{n=1}^{N} \frac{b_i^{(n)}}{s - q_n} \quad \forall i = 1, \ldots, P\,. \tag{26}$$

3. We further propose to account for multiple inputs potentially exciting the system simultaneously by applying linear superposition and expressing each output component $\widetilde{Y}_i(s)$ in terms of all input components $\widetilde{U}_j(s)$.

The above considerations lead us to parameterize and formulate the fitting condition (25) as

$$\tilde{Y}_i(s) \approx \sum_{j=1}^{P} \frac{c_{ij}^{(0)} + \sum_{n=1}^{N} \frac{c_{ij}^{(n)}}{s - q_n}}{d_0 + \sum_{n=1}^{N} \frac{d_n}{s - q_n}} \cdot \tilde{U}_j(s) + \frac{b_i^{(0)} + \sum_{n=1}^{N} \frac{b_i^{(n)}}{s - q_n}}{s \cdot \left(d_0 + \sum_{n=1}^{N} \frac{d_n}{s - q_n} \right)} \quad \forall i = 1, \dots, P. \quad (27)$$

In (27), the coefficients $c_{ij}^{(n)}$ represent the elements in the numerator $\mathbf{N}(s)$ of the small-signal model transfer function $\mathbf{H}(s)$ expressed in barycentric form. The coefficients d_n of the denominator are common to all transfer matrix entries, so that a common pole set is enforced for the model. Finally, the coefficients $b_i^{(n)}$ provide a parameterization of the zero-input response in barycentric form, as written in (25).

Multiplying both sides by the common denominator and taking the inverse Laplace transform leads to the following time-domain fitting condition for $t \geq 0$:

$$d_0 \cdot \tilde{y}_i(t) + \sum_{n=1}^{N} d_n \cdot \tilde{y}_i^{(n)}(t)$$

$$\approx \sum_{j=1}^{P} \left[c_{ij}^{(0)} \cdot \tilde{u}_j(t) + \sum_{n=1}^{N} c_{ij}^{(n)} \cdot \tilde{u}_j^{(n)}(t) \right]$$

$$+ b_i^{(0)} \cdot \Theta(t) + \sum_{n=1}^{N} b_i^{(n)} \Theta^{(n)}(t), \ \forall i = 1, \dots, P, \quad (28)$$

where $\Theta(t)$ is the Heaviside unit step function.

6. Implementation

In this section, we provide a compact and efficient formulation of the least squares formulation at the heart of the RTVF routine. Writing (28) for $t = t_k$, with $k = 1, \dots, K$, leads to the following RTVF condition in matrix form:

$$\boldsymbol{\phi}_i \cdot \boldsymbol{d} + \sum_{j=1}^{P} \boldsymbol{\psi}_j \cdot \boldsymbol{c}_{ij} + \boldsymbol{\beta} \cdot \boldsymbol{b}_i \approx \boldsymbol{0} \quad \forall i = 1, 2, \dots, P, \quad (29)$$

where the vectors collecting the unknown coefficients are

$$\boldsymbol{d} = \begin{bmatrix} d_0 \\ \vdots \\ d_N \end{bmatrix}, \ \boldsymbol{c}_{ij} = \begin{bmatrix} c_{ij}^{(0)} \\ \vdots \\ c_{ij}^{(N)} \end{bmatrix}, \ \boldsymbol{b}_i = \begin{bmatrix} b_i^{(0)} \\ \vdots \\ b_i^{(N)} \end{bmatrix}, \quad (30)$$

and where the regressor matrices collecting the filtered signal time samples (according to (5)) are defined as

$$\boldsymbol{\phi}_i = - \begin{bmatrix} \tilde{y}_i(t_1) & \tilde{y}_i^{(1)}(t_1) & \dots & \tilde{y}_i^{(N)}(t_1) \\ \vdots & \vdots & \ddots & \vdots \\ \tilde{y}_i(t_k) & \tilde{y}_i^{(1)}(t_K) & \dots & \tilde{y}_i^{(N)}(t_K) \end{bmatrix} \tag{31}$$

$$\boldsymbol{\psi}_j = \begin{bmatrix} \tilde{u}_j(t_1) & \tilde{u}_j^{(1)}(t_1) & \dots & \tilde{u}_j^{(N)}(t_1) \\ \vdots & \vdots & \ddots & \vdots \\ \tilde{u}_j(t_k) & \tilde{u}_j^{(1)}(t_K) & \dots & \tilde{u}_j^{(N)}(t_K) \end{bmatrix} \tag{32}$$

$$\boldsymbol{\beta} = \begin{bmatrix} 1 & \Theta^{(1)}(t_1) & \dots & \Theta^{(N)}(t_1) \\ \vdots & \vdots & \ddots & \vdots \\ 1 & \Theta^{(1)}(t_K) & \dots & \Theta^{(N)}(t_K) \end{bmatrix}. \tag{33}$$

Further, by defining

$$\boldsymbol{\Delta} = \begin{bmatrix} \boldsymbol{\psi}_1 & \dots & \boldsymbol{\psi}_P & \boldsymbol{\beta} \end{bmatrix}, \quad \boldsymbol{a}_i = \begin{bmatrix} \boldsymbol{c}_{i1}^T & \dots & \boldsymbol{c}_{iP}^T & \boldsymbol{b}_i^T \end{bmatrix}^T \tag{34}$$

and collecting all components, (29) reveals the bordered-block-diagonal structure of the RTVF least squares system:

$$\begin{bmatrix} \boldsymbol{\Delta} & \boldsymbol{0} & \dots & \boldsymbol{0} & \boldsymbol{\phi}_1 \\ \boldsymbol{0} & \boldsymbol{\Delta} & \dots & \boldsymbol{0} & \boldsymbol{\phi}_2 \\ \vdots & \vdots & \ddots & \vdots & \vdots \\ \boldsymbol{0} & \boldsymbol{0} & \dots & \boldsymbol{\Delta} & \boldsymbol{\phi}_P \end{bmatrix} \begin{bmatrix} \boldsymbol{a}_1 \\ \boldsymbol{a}_2 \\ \vdots \\ \boldsymbol{a}_P \\ \boldsymbol{d} \end{bmatrix} \approx \boldsymbol{0}. \tag{35}$$

Standard techniques can be employed to avoid the all-zero trivial solution, as explained in [26,35].

As in standard TDVF, once the set of unknown coefficients is found by solving (35), the zeros z_n of the denominator $D(s)$ are computed and used as initial poles for the next iteration. The process is repeated until convergence. Pseudocode for RTVF is provided in Algorithm 1. The final steps (lines 8–10) estimate the residues of a rational approximation based on the fixed poles obtained from the pole relocation process (lines 1–7). In line 10, the vector $\tilde{\boldsymbol{y}}_i$ collects all time samples of the i-th small-signal output component.

Algorithm 1 The RTVF algorithm

Input: Time samples $\boldsymbol{u}(t_k)$, $\boldsymbol{y}(t_k)$, sampling frequency F_s, starting poles $\{q_1, \dots, q_N\}$, maximum iteration number $\nu_{\max}$
Output: Estimated transfer function $\mathbf{H}(s)$
 1: Compute $\tilde{\boldsymbol{u}}(t_k) \leftarrow \boldsymbol{u}(t_k) - \boldsymbol{u}(t_1)$, $\tilde{\boldsymbol{y}}(t_k) \leftarrow \boldsymbol{y}(t_k) - \boldsymbol{y}(t_1)$
 2: **for** $\nu = 1, .., \nu_{\max}$ **do**
 3:    Compute filtered signals $\tilde{y}_i^{(n)}(t_k)$, $\tilde{u}_i^{(n)}(t_k)$, $\Theta^{(n)}(t_k)$
 4:    Build and solve the least squares problem (35)
 5:    Compute the zeros z_n of denominator $D(s)$ in (7)
 6:    Set $q_n \leftarrow z_n$
 7: **end for**
 8: Set $D(s) = 1$
 9: Compute filtered signals $\tilde{u}_i^{(n)}(t_k)$, $\Theta^{(n)}(t_k)$
10: Build matrix $\boldsymbol{\Delta}$ and solve $\boldsymbol{\Delta} \boldsymbol{a}_i \approx \tilde{\boldsymbol{y}}_i$ for $i = 1, \dots, P$
11: **return:** $\mathbf{H}(s) = \mathbf{N}(s)$, where $N_{ij}(s)$ is numerator of (6)

---

7. Numerical Results

In this section, we test RTVF in three different settings. First, we analyze its performance in the context of high order and high dimensional synthetic test systems. Next, we test its ability to model individual generator dynamics in the 39-bus system. Finally, we test its ability to model aggregated "wide area" dynamics in the 39-bus system.

7.1. Consistency

We tested the RTVF consistency by running a systematic experimental campaign over a set of synthetic randomly generated LTI reference systems, with the objective of checking whether RTVF could provide accurate estimates of all system poles. All modeled systems shared the same dynamic order of $N = 10$, but had different sizes, with P ranging from 2 to 30. The set of input-output data were generated as colored noise which showed a flat power spectrum up to angular frequency $\omega_{\max}$, where the fastest pole of the reference system appeared. The sampling frequency was fixed to $F_s = 10\,\omega_{\max}/2\pi$, and the total number of collected samples was $K = 5000$ in all cases. The modeling window started at sample $k = 250$.

Three metrics were used to assess performance of RTVF:

- the consistency of the pole estimates, as measured by the Hausdorff distance $d_H(\mathcal{P}, \mathcal{Q})$ between the set of exact poles $\mathcal{P} = \{p_1, \ldots, p_N\}$ of the true system and the set of numerically computed poles $\mathcal{Q} = \{q_1, \ldots, q_N\}$; we recall that the *Hausdorff distance* between two sets $\mathcal{P}$ and $\mathcal{Q}$ is defined as

$$d_H(\mathcal{P}, \mathcal{Q}) = \max\{\sup_{p\in\mathcal{P}} \inf_{q\in\mathcal{Q}} ||p - q||, \sup_{q\in\mathcal{Q}} \inf_{p\in\mathcal{P}} ||p - q||\}, \tag{36}$$

- the worst-case time domain output error, computed as

$$E_\infty = \max_{i=1,\ldots,P} ||\boldsymbol{y}_i - \boldsymbol{\breve{y}}_i||_\infty, \tag{37}$$

- and the RMS-normalized maximum error, computed as

$$E_\infty^{\mathrm{RMS}} = \max_{i=1,\ldots,P} \frac{||\boldsymbol{y}_i - \boldsymbol{\breve{y}}_i||_\infty}{||\boldsymbol{\breve{y}}_i||_2}. \tag{38}$$

The experiments showed that RTVF recovered the system poles almost exactly, with a set distance $d_H(\mathcal{P}, \mathcal{Q}) \leq 10^{-10}$ for all 29 test cases. Similar results were obtained from the output errors: both E_∞ and E_∞^{RMS} were less than 10^{-11}. As Figure 1 shows, there is no practical difference between the model and the output data samples. In this idealized setting, we conclude that the performance of RTVF is excellent across all investigated metrics.

To further test the consistency of RTVF, we simulated the presence of measurement noise on the input and output signals (for the case where $P = 2$, $N = 10$). Signal corruption was performed by adding a vector of zero-mean Gaussian random variables $\boldsymbol{x}_n$ to any input or output small-signal vector $\widetilde{x}$ as

$$\widetilde{x}_N = \widetilde{x} + \boldsymbol{x}_n, \tag{39}$$

with a prescribed signal to noise ratio

$$\alpha = \mathrm{SNR} = 20\log\frac{\mathrm{RMS}\{\widetilde{x}\}}{\mathrm{RMS}\{\boldsymbol{x}_n\}}. \tag{40}$$
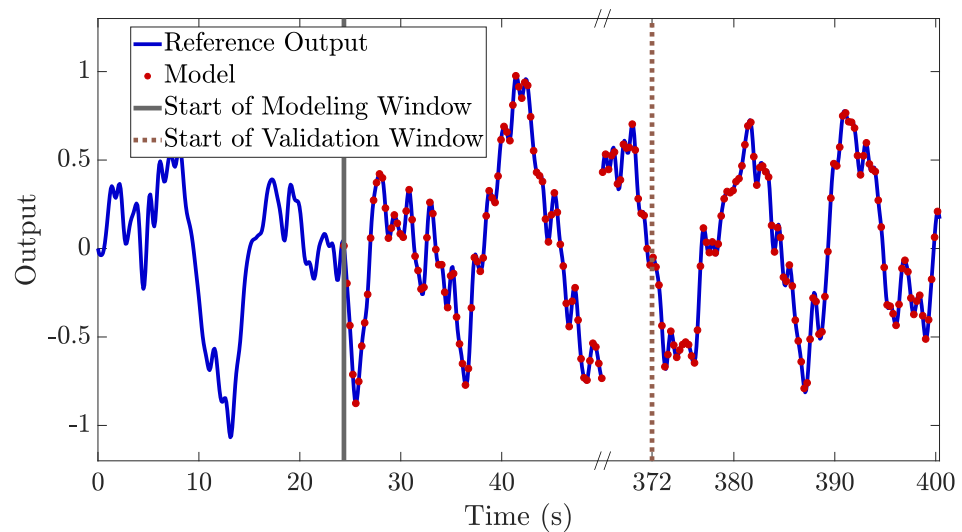
Figure 1. Time domain modeling results for a synthetic test case with $P = 2$. The modeling window starts after 24 s, the validation window starts at 372 s.

In our experiments, we considered increasing levels of SNR, ranging from 10 to 100, with resolution steps of 2. For each level of SNR, we modeled $R = 50$ different synthetic systems, and we computed the average *Signal to Error Ratio* (SER) both in time and frequency domain, which is defined as follows. Let z be a vector collecting the samples of either a reference time-domain output signal or a target frequency-domain transfer matrix element, and z_M the corresponding response of one of the R models. Then for this signal the SER is defined as

$$\text{SER} = 20 \log \frac{\text{RMS}\{z\}}{\text{RMS}\{z - z_M\}}. \tag{41}$$

For any fixed SNR level, we computed the time-domain TD-SER by averaging the performance induced by (41) over the R models and the two output signals. The frequency-domain FD-SER was computed in the same way, by averaging over the transfer matrix elements. These two metrics are shown in the top panel of Figure 2.

The meaning of the SER being above or below the black line threshold is that RTVF is either rejecting or amplifying the presence of the noise on the data, respectively. Since the TD-SER is always above the plane bisector (solid black line), RTVF is able to partially reject the presence of measurements noise in the training data. This noise rejection property is expected, since the basis functions involved in the estimation procedure effectively filter the noisy input and output signals via (5). On the other hand, FD-SER follows the bisector almost exactly, confirming also a good frequency-domain accuracy.

The noise-corrupted training input signals for a representative test case for SNR = 16 are depicted in the middle panel of Figure 2, whereas the corresponding extracted model is validated against the reference time-domain output in the bottom panel. Even with this significant amount of noise, the time-domain prediction capabilities of the model are excellent.
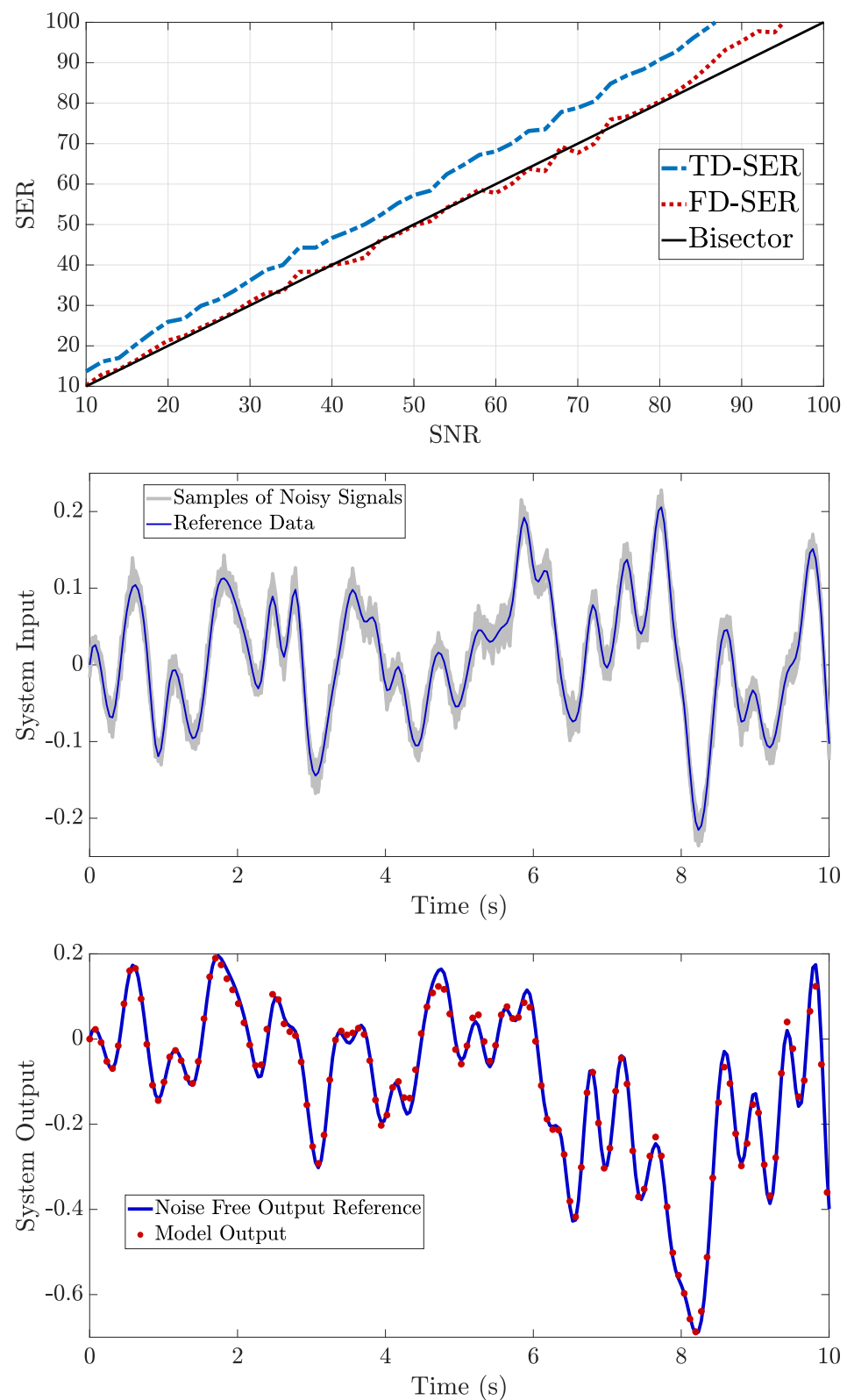
Figure 2. Top panel: the trend of TD-SER and FD-SER against the SNR. Middle panel: corrupting one training input signal (solid line) with SNR = 16 (a cloud of $R = 50$ different realizations are depicted in a grey shade). Bottom panel: response of a time domain model extracted from one noisy data realization (SNR = 16) compared to the reference noise-free signal.

7.2. Generator Modeling in the IEEE 39-Bus System

In order to test the performance of RTVF in a simulated power system setting, we collected data from time domain simulations performed on the IEEE 39-Bus New England system. This system includes 10 generators and 19 ZIP loads; the associated load, network, and generator models and numerical parameters were taken directly from [36]. Accordingly, each generator was modeled as a 6th order synchronous machine with 3rd order automatic voltage regulators and power system stabilizers; additionally, each generator was outfitted with a 3rd order turbine governor (Type I) [37]. Each generator system, with its three controllers, had a total of 15 dynamical states. The interaction between the generator, its controllers, and the network is shown in Figure 3. All time domain simulations were performed using MATLAB's DAE solver ode23t by setting relative and absolute error tolerances to 10^{-7} and 10^{-8}, respectively.
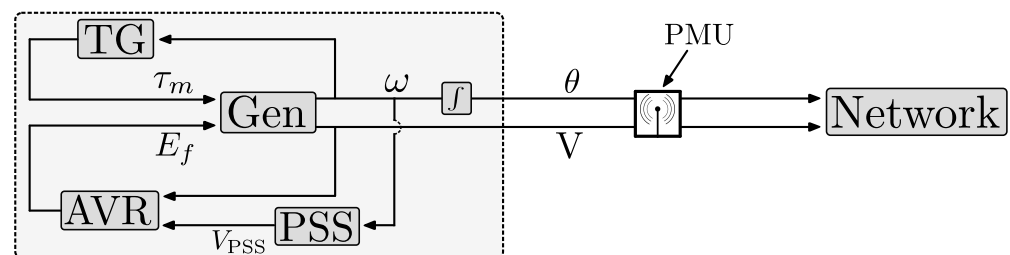
Figure 3. Shown is the interaction between the generator, its three controllers, and the network. The PMU collects data at the generator's point of connection.

Load Perturbations

In order to mimic ambient load fluctuations, we applied an Ornstein-Uhlenbeck (OU) process [38] to the active and reactive power demands at each load. The dynamics of these processes are given by $\tau \dot{u}_p = -u_p + \eta_p$ and $\tau \dot{u}_q = -u_q + \eta_q$, where η_p, η_q are zero-mean Gaussian variables, and the "load reversal" time constant τ was set to 50 s. We further applied a low-pass filter (LPF), with a cutoff frequency of ~ 9 Hz, to the OU variables such that $\hat{u} = \text{LPF}\{u\}$. This filtering operation was applied because dynamics above this frequency range become inconsistent with the quasi-stationary phasor approximation used in modeling the network's dynamics. Therefore, high frequency load behaviour is effectively neglected. Finally, these filtered OU variables were parameterized with time variable t using a cubic spline interpolation and applied to the individual ZIP loads via

$$P(t, V) = P_0 (1 + \beta \cdot \hat{u}_p(t)) (a_Z \overline{V}^2 + a_I \overline{V}^1 + a_P \overline{V}^0) \tag{42}$$

$$Q(t, V) = Q_0 (1 + \beta \cdot \hat{u}_q(t)) (b_Z \overline{V}^2 + b_I \overline{V}^1 + b_P \overline{V}^0), \tag{43}$$

where $\overline{V} \equiv V/V_0$. As a final step, scalar variable β in (42) and (43) was experimentally tuned to a numerical value of $\beta = 50$; this tuning generated load perturbations whose corresponding network voltage perturbations approximately matched those of real PMU data (in terms of signal strength).

We then applied RTVF to data measured at the machine-network interface in order to model a single generator's closed-loop dynamics. For modeling purposes, we treated voltage magnitude $V(t)$ and voltage phase $\theta(t)$ signals as inputs, and we treated current magnitude $I(t)$ and current phase $\phi(t)$ signals as outputs. The RTVF algorithm sought to generate a MIMO model with $P = 2$ and various reduced orders N.

In order to validate the quality of the model generated in the absence of measurement noise, we refer to the time and frequency domain references provided by the exact machine equations. The results are provided in Figure 4. The results show the model accuracy is excellent in both the time and frequency domains, even though the reduced model order (in this case $N = 9$) is less than the machine's true model order ($\bar{N} = 15$).
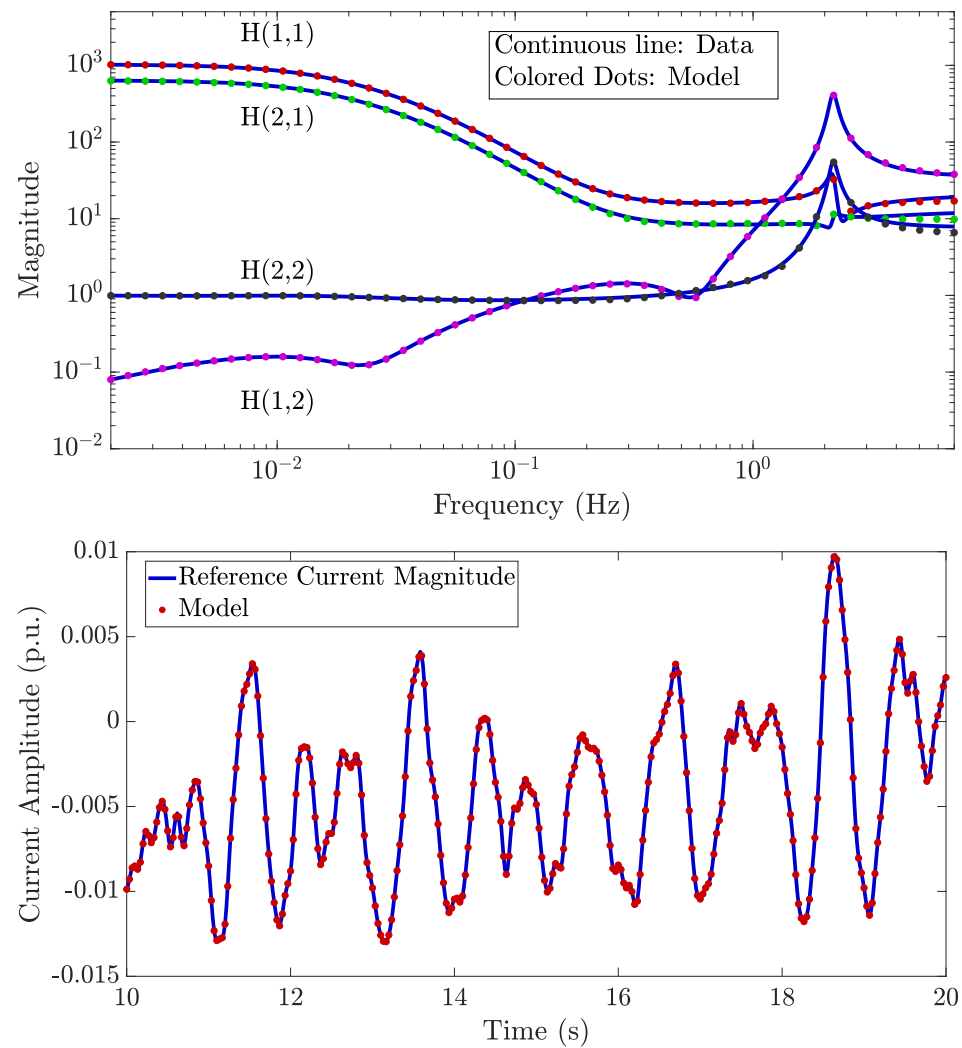
Figure 4. Noise-free generator model extraction. **Top panel**: frequency domain validation of the generator model (order $N = 9$) against exact machine equations. **Bottom panel**: the time domain validation of the model against the current magnitude reference output.

Measurement Noise

In order to further gauge the practical effectiveness of RTVF, we applied measurement noise to the voltage and current signals measured by the PMU. To apply this noise, we utilized the procedure outlined in Algorithm 2, where $\eta(t)$ represents an AWG noise vector. In this algorithm, an SNR is first specified in terms of magnitude (V, I) signals, and the proper amount of noise is then added. Next, noise with an appropriate standard deviation is applied to the phase signals (θ, ϕ), such that the total vector error (TVE) in the complex plane would be a circular cloud. In other words, an "equivalent" amount of noise is applied to both the magnitude and phase data, relative to the specified SNR value.

Top and middle panels of Figure 5 report the frequency- and time-domain fitting performance of a RTVF model of order $N = 7$ obtained for SNR = 32 dB. The corresponding noise-corrupted voltage magnitude signals are depicted in the bottom panel. Compared to the performance in the noise-free setting (Figure 4), these results show that the frequency-domain model accuracy is still quite acceptable, and that the accuracy in the time domain seems to be not affected by the presence of noise. Therefore, we conclude that the time prediction capabilities of RTVF models extracted from noisy signals are potentially adequate for power system applications.

Algorithm 2 Measurement Noise Application

Input: Voltage & current signals $V(t), I(t), \theta(t), \phi(t)$; desired SNR
Output: Noisy voltage & current signals $V_n(t), I_n(t), \theta_n(t), \phi_n(t)$
　1: $\sigma_{Vn} \leftarrow \text{RMS}\{V(t) - E\{V(t)\}\} \cdot 10^{-\text{SNR}/20}$
　2: $\sigma_{In} \leftarrow \text{RMS}\{I(t) - E\{I(t)\}\} \cdot 10^{-\text{SNR}/20}$
　3: $V_n(t) \leftarrow V(t) + \sigma_{Vn} \cdot \eta(t)$
　4: $I_n(t) \leftarrow I(t) + \sigma_{In} \cdot \eta(t)$
　5: $\theta_n(t) \leftarrow \theta(t) + \sigma_{Vn} \cdot \eta(t) / E\{V(t)\}$
　6: $\phi_n(t) \leftarrow \phi(t) + \sigma_{In} \cdot \eta(t) / E\{I(t)\}$
Return: $V_n(t), I_n(t), \theta_n(t), \phi_n(t)$

*7.3. Wide Area Monitoring in the IEEE 39-Bus System*

Finally, as a third experiment, we tested RTVF's ability to perform "wide area" monitoring in the 39-Bus system via predictive modeling. The proposed approach is here compared with the ARX modeling [21,39] and the standard Time Domain Vector Fitting scheme applied without the inclusion of initial conditions estimation. To do so, we measured the simulated current flowing across line 16–19, as shown in Figure 6, along with the voltage perturbations on bus 16. Subsequently, we used the resulting time domain data (i.e., $V(t)$, $\theta(t)$, I(t), $\phi(t)$) to model the linearized dynamics of the grey box depicted in Figure 6, consisting of two generators, a load, and their interconnecting lines. The stochastic perturbations at the load were assumed negligible, such that the observed dynamics were fully deterministic. We collected the data at a 60 Hz sampling rate for a total duration of 500 seconds, using the training subset $t \in [100, 360]$ s to generate the models using the three considered methods. The dynamics of this wide area had $\bar{N} = 30$ full order states, but using the ambient PMU data, we were able to derive a reduced order model of dynamic order $N = 13$.

The results are shown in Figure 7, where we compare the accuracy of the models in terms of output current magnitude and phase (time domain). The results we provide are referred to time domain validation data, that were not used for model generation, and that are therefore meaningful to validate the models' respective qualities; for the sake of visualization, we used a different y-axis scale for the current magnitude signal returned by the ARX model (right y-axis in the figure top panel). We observe that the proposed RTVF method outperforms ARX and TDVF algorithms, providing highly accurate predictions. We remark that, in principle, the application of TDVF in its standard formulation is not even conceivable in the considered scenario due to the presence of concurrent inputs, which were here handled by means of the proposed modified scheme of Section 6. Nevertheless, the experiments confirm that including the effect of the initial conditions is crucial to deriving a meaningful model. This is even more evident when the frequency responses of the models are compared with those of the reference system, as reported in Figure 8 for the two off-diagonal elements of the transfer matrix; the remarkable accuracy of the RTVF model is not achieved by the ARX and TDVF algorithms.
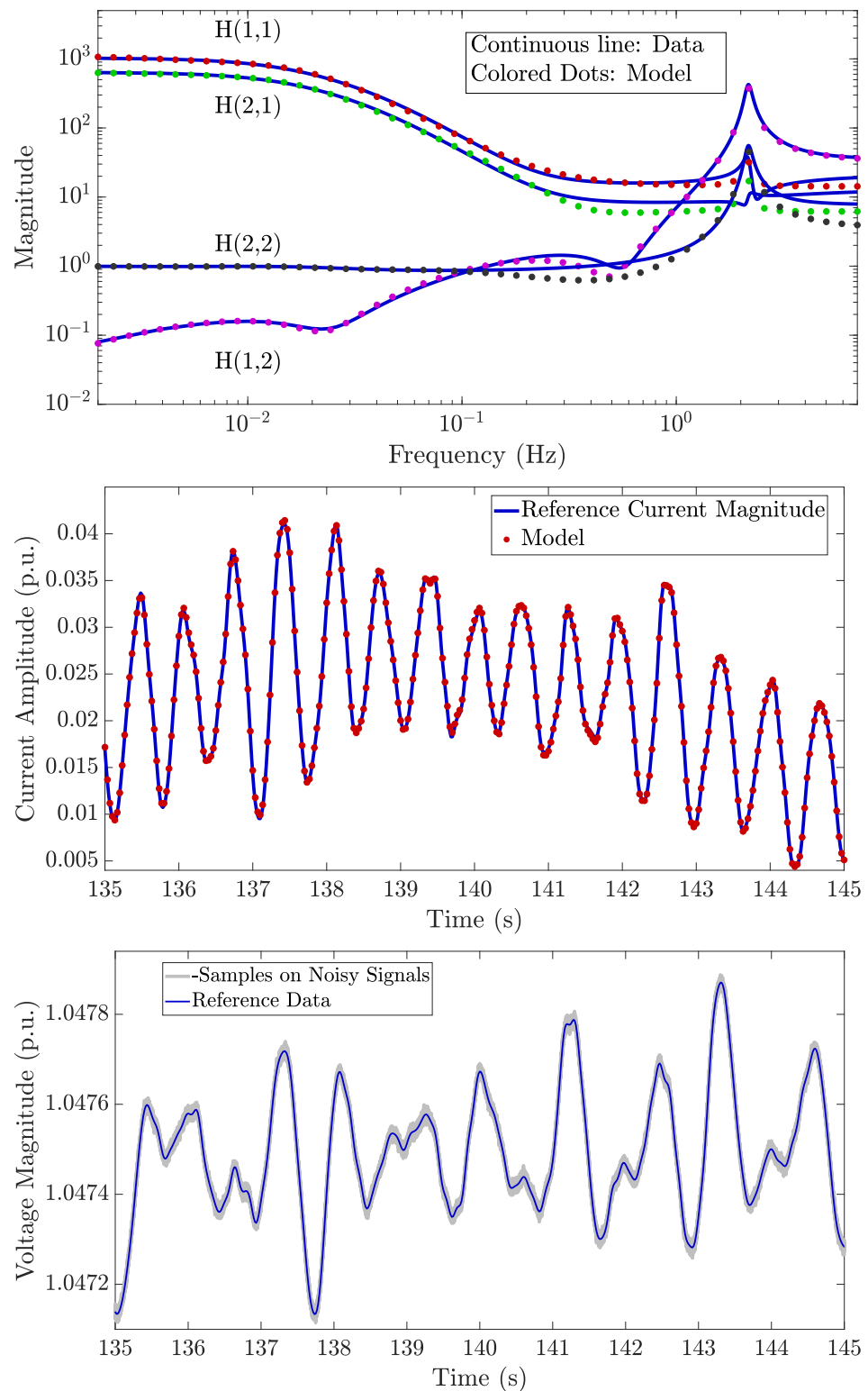
Figure 5. Generator model training from noisy data (SNR = 32). Top panel: frequency responses. Middle panel: small signal current magnitude. Bottom panel: noise-corrupted input training signals (samples from a cloud of $R = 100$ different realizations depicted with a shade of grey).

In the bottom panel, we showcase the model's excellent frequency domain accuracy by comparing it against the two off-diagonal elements of the reference transfer function. RTVF's capacity for accurately modeling aggregated power system dynamics, even at the wide area level, is clearly demonstrated by the high-fidelity results in Figures 7 and 8.
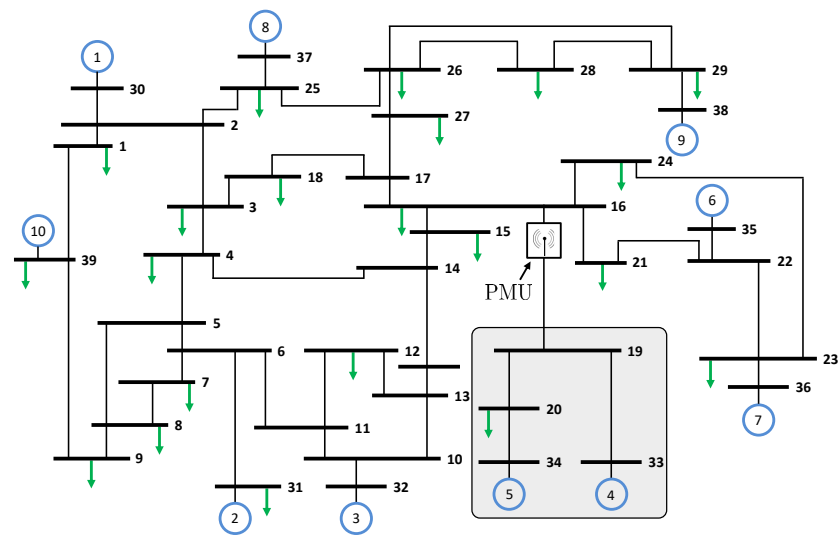
Figure 6. IEEE 39-bus New England system. The area depicted by the grey box, which geographically corresponds to a region in southern Massachusetts, US, is used to test RTVF's ability to perform wide area predictive modeling.
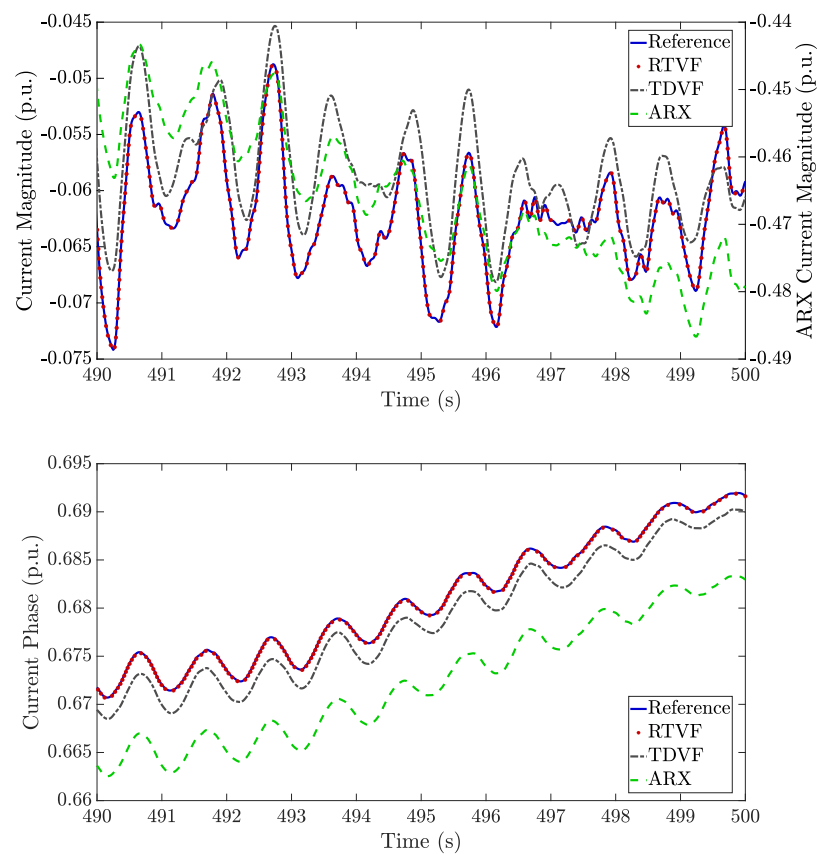
Figure 7. Wide area test case. Time domain validation of models derived by means of RTVF, ARX, and TDVF without inclusion of the initial conditions estimate. Top panel: Current magnitude deviation (note that the left y-axis applies to RTVF and TDVF, while right y-axis refers to ARX; the latter has difficulties in producing a sound approximation, especially at low frequencies). Bottom panel: Current phase deviation.
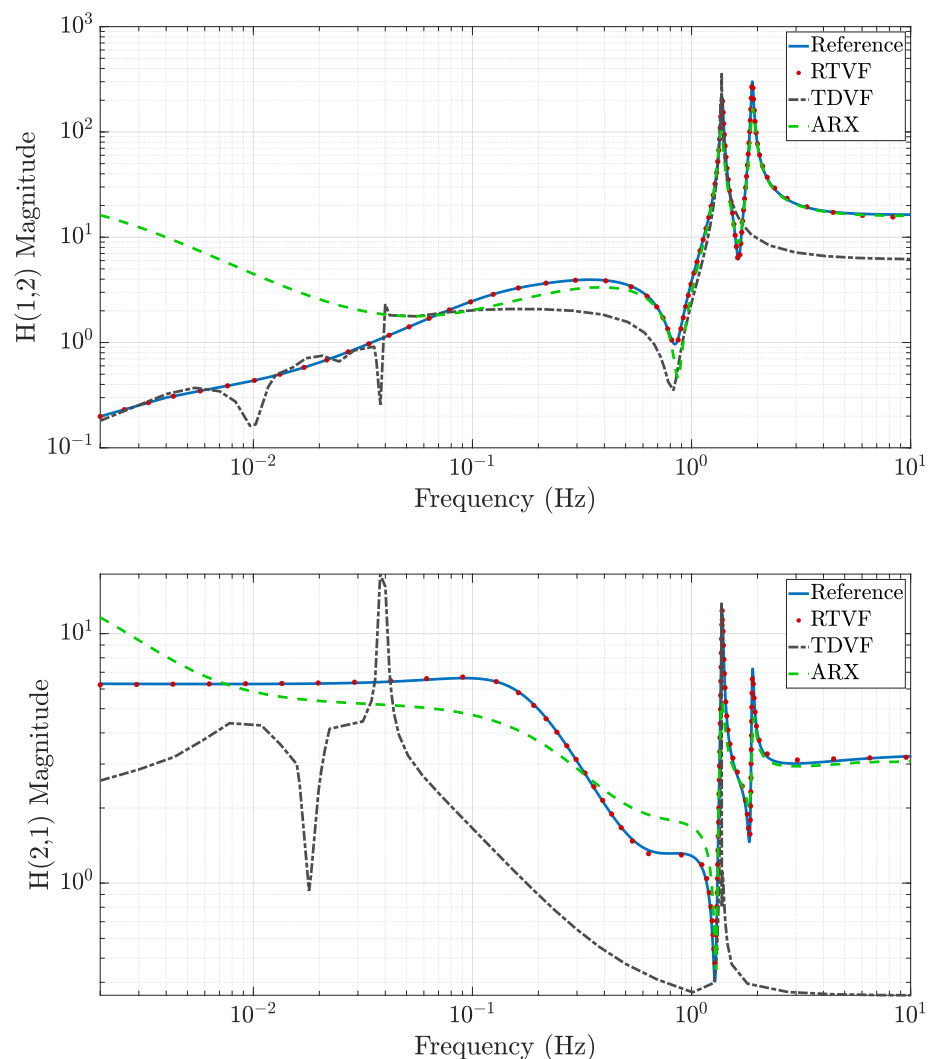
Figure 8. Selected transfer functions elements estimated by the RTVF, TDVF and ARX models, compared to the reference (exact) responses.

8. Conclusions

This work proposed a new procedure, termed Real-Time Vector Fitting (RTVF), which performs real-time predictive modeling of linearized dynamics. While the RTVF algorithm can be applied across a broad range of dynamical engineering systems, it was specifically developed to perform real-time predictive modeling of power system dynamics in the presence of ambient perturbations. Accordingly, RTVF has the following features, both of which are necessary for practical predictive modeling of power systems:

- It explicitly accounts for the presence of initial state decay in the observed output of a power system component (e.g., generator, load, or wide-area).
- It can be applied in the face of concurrently active input signals, since this is a practical constraint for any three-phase power system component modeled using a quasi-stationary phasor approximation at its terminals.

Furthermore, we compared the performance of RTVF to that of the canonical TDVF and ARX algorithms. In our experiments, the RMS error committed by RTVF on a single transfer function element was found to be about one order of magnitude smaller than what TDVF and ARX allowed for. The latter methods provide very poor prediction at lower

frequencies due to an incorrect treatment of initial state decay contributions, whereas RTVF was demonstrated to produce extremely accurate predictions over a broad frequency band.

Given the widescale deployment of PMUs and the emerging stability concerns associated with low-inertia grids, RTVF provides power system operators with a valuable tool. This tool, for example, can build real-time models of power system components whose physical prior models are unknown. It can also validate or enhance prior models which are supposedly well known. Additionally, since controller parameters (e.g., droop gain) are often changed at the local level without system operator awareness, extensions of the RTVF scheme can be used to infer the true value of these parameters in real-time, as was analogously demonstrated in [25]. Such capability can allow grid operators to maintain small-signal stability and ensure that generators are properly adhering to market regulations. To enhance its practical effectiveness, future research will couple RTVF with advanced noise filtering mechanisms. Also, physically-aware regularization techniques will be developed to allow operators to more effectively "track" a system's shifting dynamics as operating equilibriums evolve over time.

Author Contributions: Conceptualization, T.B., S.C., M.D.S., S.G.-T., L.D.; methodology, T.B., S.C., M.D.S., S.G.-T., L.D.; software, T.B., S.C., M.D.S., S.G.-T.; validation, T.B., M.D.S.; formal analysis, T.B., S.C., M.D.S., S.G.-T., L.D.; investigation, T.B., S.C., M.D.S., S.G.-T., L.D.; resources, S.G.-T., L.D.; data curation, S.C.; writing—original draft preparation, T.B., S.C., M.D.S., S.G.-T., L.D.; writing—review and editing, T.B., S.C., M.D.S., S.G.-T., L.D.; visualization, T.B., M.D.S.; supervision, S.G.-T., L.D.; project administration, S.G.-T., L.D.; funding acquisition, S.G.-T., L.D.; All authors have read and agreed to the published version of the manuscript.

Institutional Review Board Statement: Not applicable.

Informed Consent Statement: Not applicable.

Conflicts of Interest: The authors declare no conflict of interest.

Abbreviations

The following abbreviations are used in this manuscript:

WAMS	Wide Area Measurement Systems
PMU	Phasor Measurement Unit
ERCOT	Electric Reliability Council of Texas
DSA	Dynamic Security Assessment
NERC	North American Electric Reliability Corporation
PDCI	Pacific Direct Current Intertie
HVDC	High Voltage Direct Current
ARX	Autoregressive with Exogenous Input
MIMO	Multi-Input Multi-Output
RDPM	Relative Dominant-Pole Measurements
SISO	Single-Input Single-Output
TDVF	Time Domain Vector Fitting
RTVF	Real-Time Vector Fitting
LTI	Linear Time Invariant
ZIP	Impedance-Current-Power
SNR	Signal to Noise Ratio
SER	Signal to Error Ratio
RMS	Root Mean Square
DAE	Differential Algebraic Equations
LPF	Low Pass Filter
OU	Ornstein-Uhlenbeck

References

1. Vaiman, M.; Quint, R.; Silverstein, A.; Papic, M.; Kosterev, D.; Leitschuh, N.; Etingov, P. Using Synchrophasors to Improve Bulk Power System Reliability in North America. In Proceedings of the 2018 IEEE Power and Energy Society General Meeting (PESGM), Portland, OR, USA, 5–10 August 2018; pp. 1–5.
2. ERCOT. *ERCOT Nodal Operating Guides*; Technical Report; ERCOT: Austin, TX, USA, 2018.
3. Milano, F.; Dorfler, F.; Hug, G.; Hill, D.J.; Verbic, G. Foundations and Challenges of Low-Inertia Systems (Invited Paper). In Proceedings of the 2018 Power Systems Computation Conference (PSCC), Dublin, Ireland, 11–15 June 2018; pp. 1–25.
4. Quint, R. Applicable NERC Reliability Standards. Available online: https://www.nerc.com/comm/PC/Power%20Plant%20 Modeling%20and\%20Verification%20Task%20Force/Power_Plant_Model_Verification_and_Testing.pdf (accessed on 1 October 2020).
5. Akhlaghi, S.; Raheem, S.; Zhou, N. Model Validation Lessons Learned through Implementing NERC MOD-033-1. In Proceedings of the 2020 IEEE Power Energy Society General Meeting (PESGM), Montreal, QC, Canada, 2–6 August 2020; pp. 1–5. [CrossRef]
6. Li, Y.; Diao, R.; Huang, R.; Etingov, P.; Li, X.; Huang, Z.; Ning, A. An innovative software tool suite for power plant model validation and parameter calibration using PMU measurements. In Proceedings of the 2017 IEEE Power Energy Society General Meeting, Chicago, IL, USA, 16–20 July 2017; pp. 1–5.
7. Pierre, B.J.; Wilches-Bernal, F.; Schoenwald, D.A.; Elliott, R.T.; Trudnowski, D.J.; Byrne, R.H.; Neely, J.C. Design of the Pacific DC Intertie Wide Area Damping Controller. *IEEE Trans. Power Syst.* **2019**, *34*, 3594–3604. [CrossRef]
8. Trudnowski, D.; Kosterev, D.; Wold, J. Open-loop PDCI probing tests for the Western North American power system. In Proceedings of the 2014 IEEE PES General Meeting | Conference Exposition, National Harbor, MD, USA, 27–31 July 2014; pp. 1–5. [CrossRef]
9. Kundur, P. *Power System Stability and Control*; McGraw-Hill: New York, NY, USA, 1994; Volume 7.
10. Machowski, J.; Lubosny, Z.; Bialek, J.W.; Bumby, J.R. *Power System Dynamics: Stability and Control*; John Wiley and Sons: New York, NY, USA, 2020.
11. Foroutan, S.A.; Srivastava, A. Generator Model Validation and Calibration using Synchrophasor Data. In Proceedings of the 2019 IEEE Industry Applications Society Annual Meeting, Baltimore, MD, USA, 29 September–3 October 2019; pp. 1–6.
12. Huang, R.; Diao, R.; Li, Y.; Sanchez-Gasca, J.; Huang, Z.; Thomas, B.; Zhao, J. Calibrating Parameters of Power System Stability Models Using Advanced Ensemble Kalman Filter. *IEEE Trans. Power Syst.* **2018**, *33*, 2895–2905. [CrossRef]
13. Huang, Z.; Du, P.; Kosterev, D.; Yang, S. Generator dynamic model validation and parameter calibration using phasor measurements at the point of connection. *IEEE Trans. Power Syst.* **2013**, *28*, 1939–1949. [CrossRef]
14. Wu, M.; Xie, L. A Feature-Based Diagnosis Framework for Power Plant Model Validation. In Proceedings of the 2018 Power Systems Computation Conference (PSCC), Dublin, Ireland, 11–15 June 2018; pp. 1–7.
15. Pierre, J.W.; Trudnowski, D.; Donnelly, M.; Zhou, N.; Tuffner, F.K.; Dosiek, L. Overview of System Identification for Power Systems from Measured Responses1. *IFAC Proc. Vol.* **2012**, *45*, 989–1000.
16. Dosiek, L.; Zhou, N.; Pierre, J.W.; Huang, Z.; Trudnowski, D.J. Mode shape estimation algorithms under ambient conditions: A comparative review. *IEEE Trans. Power Syst.* **2013**, *28*, 779–787. [CrossRef]
17. Hauer, J.F.; Demeure, C.J.; Scharf, L.L. Initial results in Prony analysis of power system response signals. *IEEE Trans. Power Syst.* **1990**, *5*, 80–89. [CrossRef]
18. Pierre, J.W.; Trudnowski, D.J.; Donnelly, M.K. Initial results in electromechanical mode identification from ambient data. *IEEE Trans. Power Syst.* **1997**, *12*, 1245–1251. [CrossRef]
19. Wies, R.W.; Pierre, J.W.; Trudnowski, D.J. Use of ARMA block processing for estimating stationary low-frequency electromechanical modes of power systems. *IEEE Trans. Power Syst.* **2003**, *18*, 167–173. [CrossRef]
20. Dosiek, L.; Pierre, J.W. Estimating electromechanical modes and mode shapes using the multichannel ARMAX model. *IEEE Trans. Power Syst.* **2013**, *28*, 1950–1959. [CrossRef]
21. Chai, J.; Liu, Y.; Liu, Y.; Bhatt, N.; Rosso, A.D.; Farantatos, E. Measurement-based system reduction using autoregressive model. In Proceedings of the 2016 IEEE/PES Transmission and Distribution Conference and Exposition (T D), Dallas, TX, USA, 3–5 May 2016; pp. 1–5.
22. Zhang, X.; Xue, Y.; You, S.; Liu, Y.; Yuan, Z.; Chai, J.; Liu, Y. Measurement-based power system dynamic model reductions. In Proceedings of the 2017 North American Power Symposium (NAPS), Morgantown, WV, USA, 17–19 September 2017; pp. 1–6.
23. Banuelos-Cabral, E.; Nuno-Ayon, J.; Gustavsen, B. Spectral fitting approach to estimate electromechanical oscillation modes and mode shapes by using vector fitting. *Electr. Power Syst. Res.* **2019**, *176*, 105958. [CrossRef]
24. Schumacher, R.; Oliveira, G.H.; Kuiava, R. A novel time-domain linear ringdown method based on vector fitting for estimating electromechanical modes. *Electr. Power Syst. Res.* **2018**, *160*, 300–307. [CrossRef]
25. Jakobsen, S.H.; Uhlen, K. Vector fitting for estimation of turbine governing system parameters. In Proceedings of the 2017 IEEE Manchester PowerTech, Manchester, UK, 18–22 June 2017; pp. 1–6.
26. Grivet-Talocia, S.; Gustavsen, B. *Passive Macromodeling: Theory and Applications*; John Wiley and Sons: New York, NY, USA, 2016.
27. Candy, J. *Model-Based Processing*; Wiley Online Library: New York, NY, USA, 2019.
28. Jamaludin, I.W.; Wahab, N.A.; Khalid, N.S.; Sahlan, S.; Ibrahim, Z.; Rahmat, M.F. N4SID and MOESP subspace identification methods. In Proceedings of the 2013 IEEE 9th International Colloquium on Signal Processing and Its Applications, Kuala Lumpur, Malaysia, 8–10 March 2013; pp. 140–145. [CrossRef]

29. Grivet-Talocia, S. Package Macromodeling via Time-Domain Vector Fitting. *IEEE Microw. Wirel. Components Lett.* **2003**, *13*, 472–474. [CrossRef]

30. Grivet-Talocia, S. The Time-Domain Vector Fitting Algorithm for Linear Macromodeling. *Int. J. Electron. Commun. (AEU)* **2004**, *58*, 293–295. [CrossRef]

31. Harnefors, L. Modeling of Three-Phase Dynamic Systems Using Complex Transfer Functions and Transfer Matrices. *IEEE Trans. Ind. Electron.* **2007**, *54*, 2239–2248. [CrossRef]

32. Gustavsen, B.; Semlyen, A. Rational approximation of frequency domain responses by vector fitting. *Power Deliv. IEEE Trans.* **1999**, *14*, 1052–1061. [CrossRef]

33. Lefteriu, S.; Antoulas, A.C. On the Convergence of the Vector-Fitting Algorithm. *Microw. Theory Tech. IEEE Trans.* **2013**, *61*, 1435–1443. [CrossRef]

34. Bradde, T.; Grivet-Talocia, S.; Calafiore, G.C.; Proskurnikov, A.V.; Mahmood, Z.; Daniel, L. Bounded Input Dissipativity of Linearized Circuit Models. *IEEE Trans. Circuits Syst. I Regul. Pap.* **2020**, *67*, 2064–2077. [CrossRef]

35. Gustavsen, B. Improving the pole relocating properties of vector fitting. *Power Deliv. IEEE Trans.* **2006**, *21*, 1587–1592. [CrossRef]

36. Hiskens, I. IEEE PES Task Force on Benchmark Systems for Stability Controls. Technical Report. 2013. Available online: http://www.sel.eesc.usp.br/ieee/IEEE39/New_England_Reduced_Model_(39_bus_system)_MATLAB_study_report.pdf (accessed on 1 May 2020).

37. Milano, F. Power System Analysis Toolbox Reference Manual for PSAT Version 2.1.8. 2013. Available online: http://faraday1.ucd.ie/psat.html (accessed on 1 May 2020).

38. Milano, F.; Zarate-Minano, R. A Systematic Method to Model Power Systems as Stochastic Differential Algebraic Equations. *IEEE Trans. Power Syst.* **2013**, *28*, 4537–4544. [CrossRef]

39. Stoica, P.; Moses, R.L. *Spectral Analysis of Signals*; Prentice-Hall: Upper Saddle River, NJ, USA, 2005.